Glucosamine improves survival in a mouse model of sepsis and attenuates sepsis-induced lung injury and inflammation

Received for publication, June 27, 2018, and in revised form, November 11, 2018 Published, Papers in Press, November 19, 2018, DOI 10.1074/jbc.RA118.004638

Ji-Sun Hwang[‡1], **Kyung-Hong Kim**[‡1], **Jiwon Park**[‡], **Sang-Min Kim**[‡], **Hyeongjin Cho**[§], **Yunkyoung Lee**[‡2], **and Inn-Oc Han**[‡2,3]

From the [‡]*Department of Physiology and Biophysics, College of Medicine, and the* [§]*Department of Chemistry, Inha University, Incheon, Korea*

Edited by Gerald W. Hart

The aim of the current study was to investigate the effects of glucosamine (GlcN) on septic lethality and sepsis-induced inflammation using animal models of mice and zebrafish. GlcN pretreatment improved survival in the cecal ligation and puncture (CLP)-induced sepsis mouse model and attenuated lipopolysaccharide (LPS)-induced septic lung injury and systemic inflammation. GlcN suppressed LPS-induced M1-specific but not M2-specific gene expression. Furthermore, increased expressions of inflammatory genes in visceral tissue of LPS-injected zebrafish were suppressed by GlcN. GlcN suppressed LPS-induced activation of mitogen-activated protein kinase (MAPK) and NF-κB in lung tissue. LPS triggered a reduction in *O*-GlcNAc levels in nucleocytoplasmic proteins of lung, liver, and spleen after 1 day, which returned to normal levels at day 3. GlcN inhibited LPS-induced *O*-GlcNAc down-regulation in mouse lung and visceral tissue of zebrafish. Furthermore, the *O*-GlcNAcase (OGA) level was increased by LPS, which were suppressed by GlcN in mouse and zebrafish. OGA inhibitors suppressed LPS-induced expression of inflammatory genes in RAW264.7 cells and the visceral tissue of zebrafish. Stable knockdown of Oga via short hairpin RNA led to increased inducible nitric oxide synthase (iNOS) expression in response to LPS with or without GlcN in RAW264.7 cells. Overall, our results demonstrate a protective effect of GlcN on sepsis potentially through modulation of *O*-GlcNAcylation of nucleocytoplasmic proteins.

Sepsis, one of the most fatal diseases worldwide, often leads to multiple organ failure, mainly due to uncontrolled inflammatory responses. However, the pathophysiological mechanisms associated with development and therapeutic targets of sepsis are largely unknown at present (1). Sepsis is often associated with organ dysfunction induced by dysregulation of host defense against infection. The lung is the most vulnerable and critical organ during sepsis (2), with acute lung injury (ALI)[4] being a common sepsis-induced inflammatory disorder (3). Lipopolysaccharide (LPS), a component of Gram-negative bacterial endotoxin that induces acute inflammation by stimulating host cells to produce proinflammatory cytokines, is recognized as the main cause of ALI (4, 5). LPS induces ALI in animal models by promoting pulmonary microvascular permeability and recruiting activated neutrophils and macrophages to the lung (6). The LPS-induced ALI mouse model is widely used for pathogenesis studies and drug development at present (7).

Macrophages circulating in blood or residing in tissues represent the first barrier against external infection through controlling both innate and acquired immunity. Because of their diversity and plasticity, macrophages undergo heterogeneous activation and polarization. Classically activated M1 and alternatively activated M2 phenotypes of macrophages represent two distinct states of activation and M1/M2 polarization is a tightly coordinated process. M1 macrophages release proinflammatory molecules such as IL-1, IL-6, TNF-α, and reactive nitrogen and oxygen intermediates, which cause tissue damage, whereas M2 macrophages release anti-inflammatory cytokines that promote wound healing and tissue repair (8).

Nitric oxide (NO), an inflammatory mediator produced by diverse immune cell types, plays a crucial role in control of host defense response to bacterial infection. iNOS expression and production of nitric oxide (NO) contribute to the pathophysiologic features of ALI (9). NF-κB, a major transcription factor of iNOS/NO regulation, normally exists in an inactive form in the cytoplasm bound to inhibitor κB (IκB). Activation of the IκB kinase complex results in phosphorylation of IκB, leading to proteolytic degradation and thereby facilitating translocation of NF-κB complexes into the nucleus. Translocated homo- or heterodimers of NF-κB subunits trigger the expression of various inflammatory target genes that are implicated in lung inflammation (10, 11). Mitogen-activated protein (MAP) kinases and AKT (also known as protein kinase B) are threonine/serine kinases that

This work was supported by National Research Foundation (NRF) of Korea Grants NRF-2017R1A2B2007199, NRF-2016R1D1A1B03934289, and NRF-2017R1C1B1007283 and a WCSL (World Class Smart Lab) research grant of Inha University. The authors declare that they have no conflicts of interest with the contents of this article.

This article contains Figs. S1–S5.

[1] Both authors should be considered as joint first authors.

[2] Both authors should be considered as joint senior authors.

[3] To whom correspondence should be addressed: Dept. of Physiology and Biophysics, College of Medicine, Inha University, 100 Inha Ro, Nam-gu, Incheon 22212, Korea. Tel.: 82-32-860-9854; Fax: 82-32-860–9851; E-mail: iohan@inha.ac.kr.

[4] The abbreviations used are: ALI, acute lung injury; LPS, lipopolysaccharide; IL, interleukin; IFN, interferon; TNF, tumor necrosis factor; CLP, cecal ligation and puncture; OGT, *O*-GlcNAc transferase; OGA, *O*-GlcNAcase; BMDM, bone marrow-derived monocyte; NO, nitric oxide; ERK, extracellular signal-regulated kinase; HAT, histone acetyltransferase; shRNA, short hairpin RNA; H&E, hematoxylin and eosin; DAPI, 4′,6-diamidino-2-phenylindole; GAPDH, glyceraldehyde-3-phosphate dehydrogenase; MAPK, mitogen-activated protein kinase; COX, cyclooxygenase.

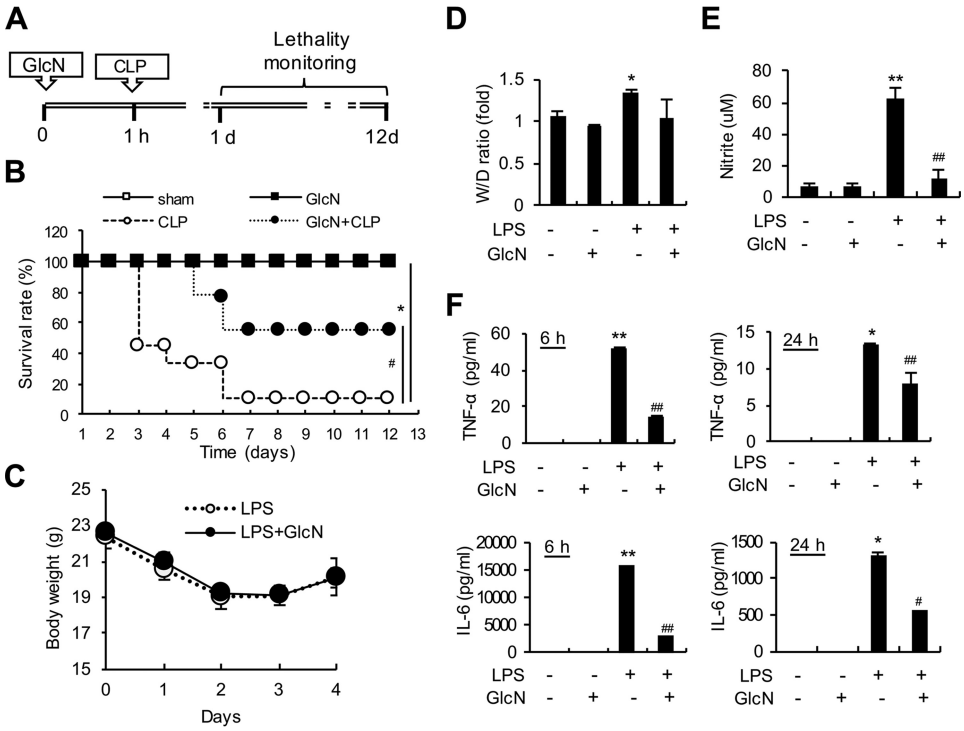

Figure 1. Effects of GlcN on survival and systemic inflammation in septic mice. *A*, schematic design of the experimental procedure. Mice ($n = 10$, each group) underwent sham or CLP operation on day 0. At 1 h before surgery, mice were subjected to intraperitoneal injection with GlcN (200 mg/kg) or PBS. *B*, survival of control and GlcN-treated septic mice was recorded over 12 days. *C–F*, mice were subjected to intraperitoneal injection with LPS (5 mg/kg body weight) with or without intraperitoneal GlcN (200 mg/kg) pre-treatment. Body weights were measured and plotted every day for 4 days after LPS injection (*C*). Pulmonary edema formation was measured via determination of the wet-to-dry (*W/D*) lung weight ratio at 24 h of LPS and/or GlcN injection (*D*). Levels of nitrite in plasma after 24 h LPS and/or GlcN challenge were measured with the Griess assay (*E*). Concentrations of TNF-α and IL-6 in plasma at 6 and 24 h of LPS and/or GlcN injection were determined using ELISA (*F*). All values are presented as mean ± S.E. *Asterisks* denote significantly increased from untreated control (*, $p < 0.05$; **, $p < 0.01$); *hash marks* indicate significantly decreased from LPS-stimulated conditions (#, $p < 0.05$; ##, $p < 0.01$).

play critical roles in inflammation through regulation of NF-κB-dependent gene transcription (12, 13).

Animal models of sepsis can provide significant insights into the complex pathophysiology of the disease. The most popular preclinical sepsis model involves mice. Various mice models with different paradigms have been generated, among which endotoxin, bacterial infusion, cecal ligation and puncture, and colon ascendens stent peritonitis models are the most commonly used (14). Zebrafish has additionally recently been reported as an excellent model to investigate innate immune responses, infectious diseases, inflammatory disorders, and other immune-related diseases (15, 16) because these animals share common major blood lineages (17) and a remarkably similar immune system with mammals (18, 19).

O-Linked GlcNAc (*O*-GlcNAc), a post-translational modification of serine and threonine residues in nuclear, cytoplasmic, and mitochondrial proteins, is an important mechanism involved in regulation of various cellular functions (20). *O*-GlcNAcylation is a dynamic and reversible process regulated by two key enzymes: *O*-GlcNAc transferase (OGT) that catalyzes the addition of *O*-GlcNAc to the hydroxyl group of serine or threonine residues of proteins and *O*-GlcNAcase (OGA) that removes *O*-GlcNAc from proteins (21). The dynamic modulation of *O*-GlcNAcylation levels on proteins results from the concerted action of these two antagonist enzymes (22). Protein *O*-GlcNAcylation is reported to play roles in transcription, cell signaling, and metabolism. Recent studies further suggest that *O*-GlcNAcylation is involved in the regulation of inflammation and exerts protective effects against inflammation-induced tissue injury, both in the brain and peripheral system (23–26). In particular, our group demonstrated that glucosamine (GlcN) exerts neuroprotective effects in a rat middle cerebral artery occlusion ischemia model through a mechanism involving a delay in damage processes via regulation of *O*-GlcNAcylation of NF-κB/P65 in the post-ischemic brain (26).

In the current study, we showed that GlcN protects against lethal septic shock and sepsis-induced lung inflammation and injury in mouse and zebrafish models and examined the potential underlying mechanisms. Notably, sepsis stimulation induced a decrease in *O*-GlcNAcylation accompanied by increased OGA expression in the lung. Based on the findings, we hypothesize that sepsis-induced hypo-*O*-GlcNAcylation of lung tissue proteins is an important injury response and restoration of *O*-GlcNAcylation by GlcN or OGA inhibitors may present important therapeutic strategies for sepsis-induced injury of lung.

Results

GlcN pretreatment decreases mortality and systemic inflammation in septic mice

To examine the effects of GlcN on septic mortality, we monitored mouse survival after cecal ligation and puncture (CLP) with or without GlcN (200 mg/kg) for 12 days (Fig. 1*A*). Based on Kaplan-Meier survival curves, mice with CLP-induced sepsis pre-

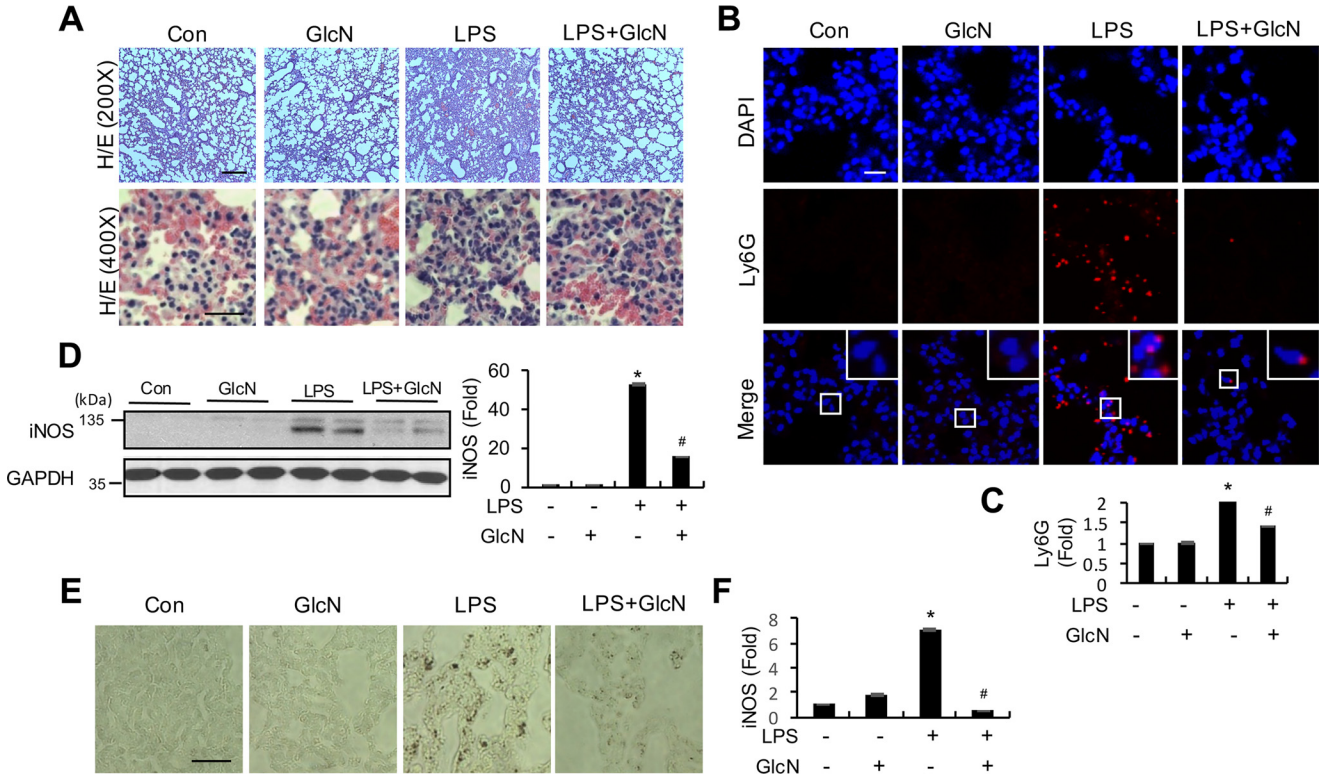

Figure 2. Effects of GlcN on pulmonary inflammation in LPS-induced septic mice. *A,* representative histological analysis of lung of control (PBS-injected) and 5 mg/kg of LPS- and/or 200 mg/kg of GlcN-injected mice via H&E staining. *Scale bar*, 500 μm (*upper*) and 200 μm (*lower*). *B* and *C,* representative immunofluorescence staining (*B*) and quantification (*C*) of lung sections from PBS-, GlcN-, LPS-, and LPS + GlcN-treated mice at 24 h for detection of LY6G (*red*) and DAPI (*blue*) signals. *Scale bar*, 200 μm. *D,* representative Western blotting of iNOS and densitometric measurement in mice lung tissue at 24 h after LPS- and/or GlcN injection. GAPDH was determined as the loading control. *E* and *F,* representative immunohistochemistry (*E*) and quantification (*F*) in mice lung tissue at 24 h after LPS- and/or GlcN injection. *Scale bar*, 200 μm. All values are presented as mean ± S.E. *Asterisk* denotes significantly increased from the untreated control ($p < 0.05$); *hash mark* (#) indicates significantly decreased from LPS-stimulated conditions ($p < 0.05$).

sented a 12-day survival rate of 11%. GlcN pretreatment increased the 12-day survival rate to 55% relative to that in mice with untreated sepsis (Fig. 1*B*). All sham-operated control mice treated with or without GlcN survived. We additionally examined the effects of GlcN pretreatment on LPS-induced sepsis. Intraperitoneal injection of LPS (5 mg/kg) did not cause death in mice for 12 days, but animals appeared very sick for the first 3–4 days with little movement. Mice with LPS-induced CLP with or without GlcN pretreatment demonstrated weight loss for the first 3 days, followed by recovery of weight (Fig. 1*C*). Estimation of the lung wet/dry weight ratios revealed that LPS-induced pulmonary edema is not significantly altered by GlcN (Fig. 1*D*). We further assessed plasma NO levels by measuring nitrite, a stable end product of NO, in mice treated with LPS and/or GlcN. Our data showed a dramatic increase in nitrite levels in serum of LPS-treated mice, which was decreased upon GlcN pretreatment (Fig. 1*E*). Plasma levels of cytokines, TNF-α and IL-6, were also strongly increased after 6 and 24 h from LPS stimulation relative to those measured in saline-injected control mice. GlcN pretreatment reduced the LPS-induced increase in TNF-α and IL-6 in plasma (Fig. 1*F*).

GlcN pretreatment suppresses histological changes, neutrophil infiltration, and iNOS gene expression in lungs of LPS-induced septic mice

Histological changes in lungs of septic mice with or without GlcN pretreatment were examined using H&E staining. One day after saline injection, lung tissues from mice in the control group displayed normal alveolar walls and no inflammatory cell infiltration. In comparison, the 5 mg/kg of LPS injection group showed obvious alveolar wall thickening (Fig. 2*A*, *upper panels*) with profound inflammatory cell infiltration (Fig. 2*A*, *lower panels*). For investigation of neutrophil and/or monocyte infiltration, lung tissues of LPS-induced septic mice with or without GlcN at 24 h were immunostained using a Ly6G antibody. LPS induced an increase in immunofluorescence, which was suppressed with GlcN pretreatment (Fig. 2, *B* and *C*). Next, we examined iNOS protein expression in lung tissue of LPS-induced septic mice with or without GlcN preincubation at 24 h. Western blotting analyses revealed a dramatic increase in iNOS protein levels in lung tissue of septic mice, which were reduced by GlcN pretreatment (Fig. 2*D*). Immunohistochemical staining disclosed significant up-regulation of iNOS in alveolar walls after exposure to LPS, which was effectively inhibited upon pretreatment with 200 mg/kg of GlcN (Fig. 2, *E* and *F*).

GlcN pretreatment inhibits expression of LPS-induced M1-typical genes in bone marrow-derived macrophage and lung tissue

Macrophages are classified into two groups, specifically, classically activated (M1) and alternatively activated (M2) cells. We further investigated whether GlcN affects LPS-induced polarization of macrophages into the proinflammatory M1 phenotype in bone marrow-derived monocytes (BMDM) and lung tissue. Our experiments revealed that GlcN pretreatment

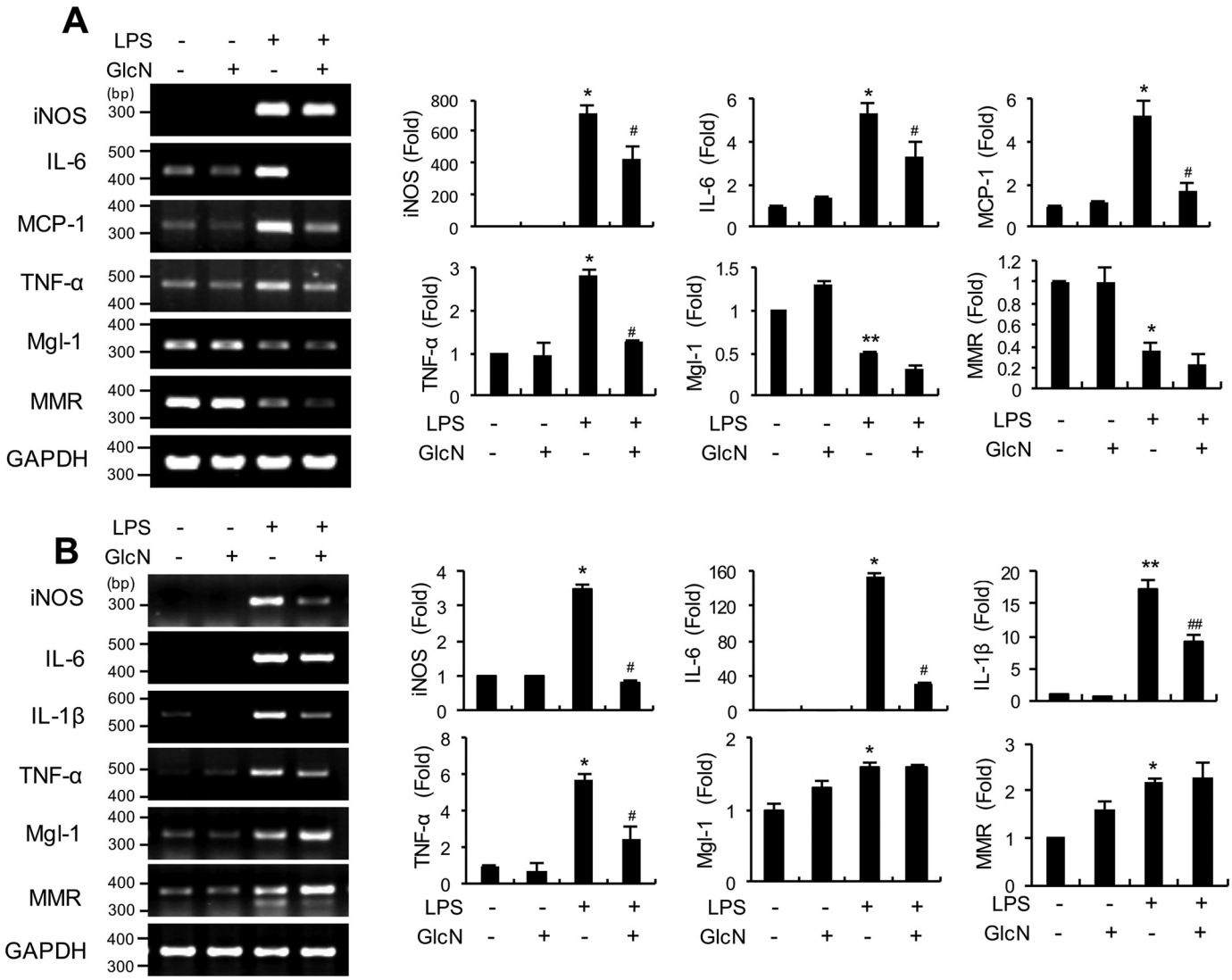

Figure 3. mRNA levels of M1/M2 macrophage markers in bone marrow cells and lung tissue of LPS- and/or GlcN-injected mice. Mice were intraperitoneally injected with GlcN (200 mg/kg) or PBS before LPS (5 mg/kg) injection. At 24 h, total mRNAs were prepared from bone marrow cells (*A*) and lung tissue (*B*). Determination of *iNos*, *Il-6*, *Mcp-1*, *Tnf-α*, *Mgl-1*, and *Mmr* mRNA levels using PCR or quantitative real-time PCR. Blots are representative of three independent experiments. All values are mean ± S.E. *Asterisks* denote significantly increased from the untreated control (*, $p < 0.05$; **, $p < 0.01$); *hash marks* indicate significantly decreased from LPS-stimulated conditions (#, $p < 0.05$; ##, $p < 0.01$).

decreased mRNA expression of LPS-induced genes encoding typical M1 genes, including *iNos*, *Il-6*, *Mcp-1*, and *Tnf-α*, in BMDM (Fig. 3*A*). LPS treatment additionally led to decreased mRNA levels of typical M2 (galactose-type C-type lectin (*Mgl-1*) and C-type mannose receptor 1 (*Mmr*)) in BMDM, which were not significantly affected by GlcN (Fig. 3*A*). We then investigated the effect of GlcN on IL-4-induced M2 polarization in BMDM cells. IL-4 treatment led to increased mRNA expression of M2 marker, including *Mgl-1*, *Arg-1*, and *Relma* (resistin-like molecule α) but GlcN did not affect gene expression of M2 signature genes (Fig. S1).

Next we examined the mRNA expressions of M1 or M2 signature genes in lung tissue of LPS- and/or GlcN-treated mice (Fig. 3*B*). Consistent with the results obtained using BMDM cells, LPS treatment led to increased levels of typical M1 genes, including *iNos*, *Il-6*, *Il-1β*, and *Tnf-α* in the lung (Fig. 3*B*). Notably, GlcN pretreatment suppressed the expression levels of these genes in lung tissue, compared with the LPS group. Pulmonary expression of M2 signature genes, *Mgl-1* and *Mmr* were increased by LPS, which were not significantly affected by GlcN pretreatment.

GlcN pretreatment inhibits mRNA expression of LPS-induced inflammatory genes in visceral tissue of zebrafish

Zebrafish has been recently proposed as an appropriate animal model to study the sepsis response or acute inflammatory conditions (27). Injection of adult zebrafish (*Danio rerio*) with LPS at concentrations of 100, 500, 1000, and 2000 μg/g of body weight resulted in no mortality (Fig. S2). To examine the inflammatory response and potential effects of GlcN on inflammation in response to LPS, zebrafish were injected with LPS (100 μg/g) with or without GlcN pretreatment. Notably, mRNA levels of inflammatory genes, including *inos*, *cox-2*, *il-1β*, *il-6*, *tnf-α*, and *ifn-γ*, were significantly elevated by LPS in visceral tissue of zebrafish. GlcN suppressed the LPS-induced elevation of these genes (Fig. 4).

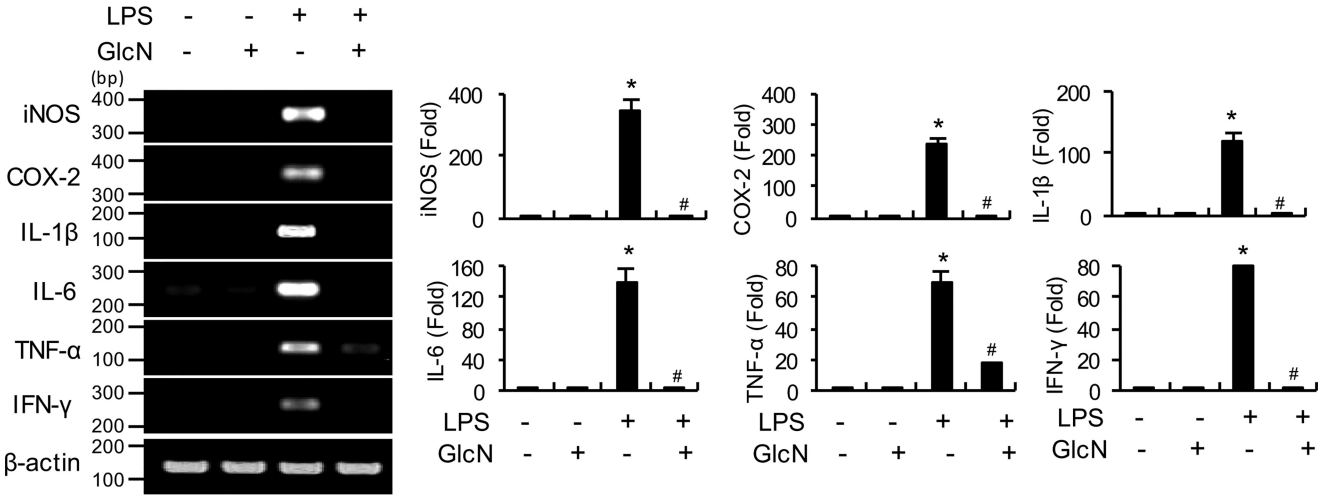

Figure 4. Levels of proinflammatory gene transcripts in visceral tissue of LPS- and/or GlcN-injected adult zebrafish. Adult zebrafish were incubated with GlcN (1 g/liter of maintained water) for 12 h before abdominal GlcN (200 μg/g) injection and subsequently stimulated with LPS (100 μg/g). Visceral tissue was separated at 24 h and *inos*, *cox-2*, *il-1β*, *il-6*, *tnf-α*, and *ifn-γ* mRNA levels were determined via PCR or quantitative real-time PCR. Blots are representative of three independent experiments. All values are mean ± S.E. *Asterisk* denotes significantly increased from the untreated control ($p < 0.05$); *hash mark* (#) indicates significantly decreased from LPS-stimulated conditions ($p < 0.05$).

GlcN suppresses MAPKs, AKT, P65, and IκB signaling in lungs of septic mice

To elucidate the molecular mechanisms underlying the anti-inflammatory effects of GlcN, we examined the signaling pathways involving mitogen-activated protein kinases (MAPK), AKT, and NF-κB in the lungs of septic mice with or without GlcN. As shown in Fig. 5*A*, phosphorylation levels of ERK, P38, JNK, and AKT were significantly increased in lung samples of LPS-treated mice, compared with the control group. The LPS + GlcN group displayed decreased pulmonary MAPK and AKT phosphorylation, compared with the LPS group (Fig. 5*A*). Furthermore, immunofluorescence staining revealed increased pulmonary expression of *p*-IκBα and *p*-P65 in LPS-treated mice, compared with control mice, which was significantly decreased in the GlcN pretreatment group (Fig. 5, *B* and *C*). Consistently, protein expression of P-IκBα was increased in the lung tissue of LPS-treated mice, which was suppressed upon GlcN pretreatment (Fig. 5*D*).

LPS induces dynamic changes in O-GlcNAcylation in lung, liver, and spleen of mice

Next, we determined time course, histological, and *O*-GlcNAcylation changes in lungs of septic mice. First, histological changes in lung at 1, 3, and 5 days were examined via H&E staining. Lung tissues from mice in the control group showed normal alveolar walls, whereas the LPS injection group displayed apparent alveolar wall thickening at day 1 and extreme thickening with profound cell infiltration at days 3 and 5 (Fig. 6*A*). We subsequently investigated the time course of *O*-GlcNAcylation changes in nucleocytoplasmic proteins in the lung via Western blotting using the anti-*O*-GlcNAc antibody (CTD110.6). LPS stimulation induced an initial dramatic decrease 1 day after injection, followed by recovery at day 3 and a further increase at day 5 (Fig. 6*B*). Examination of the time course of *O*-GlcNAcylation changes in the liver and spleen of septic mice revealed similar results to those from lung (Fig. 6*B*). *O*-GlcNAcylation after 10 min and 6 h of LPS treatment was not significantly changed in the lung tissue (Fig. S3). The consistent patterns of transient reduction followed by recovery to control (or higher) levels in the intestinal tissues of septic mice suggest that metabolic changes or enzymatic regulation of *O*-GlcNAcylation potentially play an important role in LPS-mediated inflammation and recovery.

GlcN pretreatment ameliorates sepsis-induced decrease in O-GlcNAcylation and increase in OGA expression in lungs of septic mice

We examined pulmonary changes in *O*-GlcNAcylation, OGT, and OGA in response to LPS with or without GlcN pretreatment. Western blotting results demonstrated that LPS decreases *O*-GlcNAcylation in lung after 24 h. The GlcN-pretreated LPS group displayed significantly increased *O*-GlcNAcylation, compared with the LPS group (Fig. 7*A*). Next, pulmonary expression of the two *O*-GlcNAc-processing enzymes, OGT and OGA, was evaluated in response to LPS with or without GlcN. On a Western blotting, LPS increased OGA but induced no significant changes in OGT protein expression in the lung of LPS-treated mice (Fig. 7*A*). GlcN decreased the LPS-induced increase in OGA expression, which was still higher than the control level (Fig. 7*A*). Consistently, immunofluorescence staining data showed that CLP induces a decrease in *O*-GlcNAcylation and increase in OGA expression in lung of septic mice, which can be significantly inhibited by GlcN (Fig. 7*B*). OGT expression in lung tissue was not markedly altered by CLP and/or GlcN (Fig. 7*B*).

GlcN pretreatment ameliorates the LPS-induced decrease in O-GlcNAcylation and increase in OGA expression in visceral tissue of zebrafish

We investigated the changes in *O*-GlcNAcylation, OGT, and OGA expression induced by LPS and/or GlcN in the zebrafish LPS model. To this end, adult zebrafish were injected with LPS with or without GlcN pretreatment, and *O*-GlcNAcylation, OGT, and OGA levels were measured in vis-

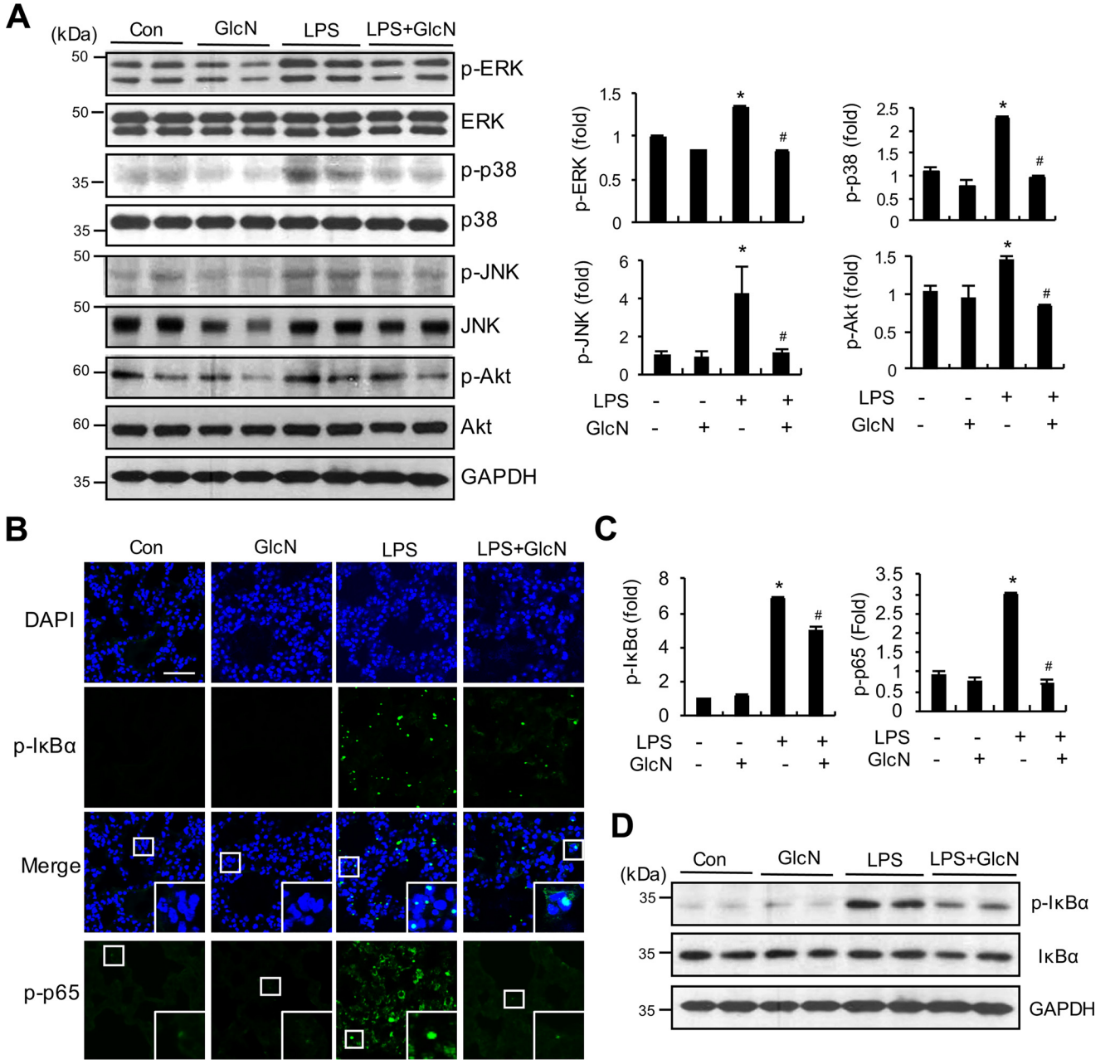

Figure 5. Effects of GlcN on LPS-induced activation of MAPKs, AKT, and IκB. Lung samples were isolated from PBS or LPS (5 mg/kg)- and/or GlcN (200 mg/kg)-injected mice at 24 h. *A,* whole lung lysates were prepared and immunoblotted with ERK, P38, JNK, AKT, *p*-ERK, *p*-P38, *p*-JNK, and *p*-AKT antibodies. Relative densitometric intensities for P-ERK, P-JNK1, and P-AKT were quantitatively measured by normalizing to ERK, P38, JNK, and AKT levels, respectively. *B* and *C,* representative confocal immunofluorescence staining images of P-IκBα and *p*-P65 are shown. Nuclei were counterstained with DAPI for visualization in lung tissue (*B*). *Scale bar*, 500 μm. Positive staining for *p*-IκBα and *p*-P65 was quantitatively assessed (*C*). *D*, Western blot analysis of *p*-IκBα, IκBα, and GAPDH proteins from whole lung lysates. Blots and fluorescent images are representative of three independent experiments. All values are presented as mean ± S.E. *Asterisk* denotes significantly increased from the untreated control ($p < 0.05$); *hash mark* (#) indicates significantly decreased from LPS-stimulated conditions ($p < 0.05$).

ceral tissue of via immunofluorescent staining. As shown in Fig. 8, *O*-GlcNAcylation was increased by GlcN but suppressed by LPS, compared with the control group. GlcN pretreatment led to recovery of the LPS-induced decrease in *O*-GlcNAcylation to the level of the control group. Furthermore, consistent with the results obtained using mice, OGA levels were significantly increased by LPS and these effects of LPS were inhibited by GlcN pretreatment (Fig. 8). The OGT level was not significantly altered by LPS and/or GlcN.

LPS and/or GlcN dynamically regulate O-GlcNAcylation in RAW264.7 cells and OGA inhibitors inhibit the LPS-induced increase in inflammatory genes in RAW264.7 cells and visceral tissue of zebrafish

Next, we investigated *O*-GlcNAcylation changes in nucleocytoplasmic proteins of RAW264.7 cells in response to LPS and/or GlcN via Western blotting and galactosyltransferase labeling. Specifically, RAW264.7 cells were stimulated with LPS with or without GlcN for 24 h. LPS induced a decrease in

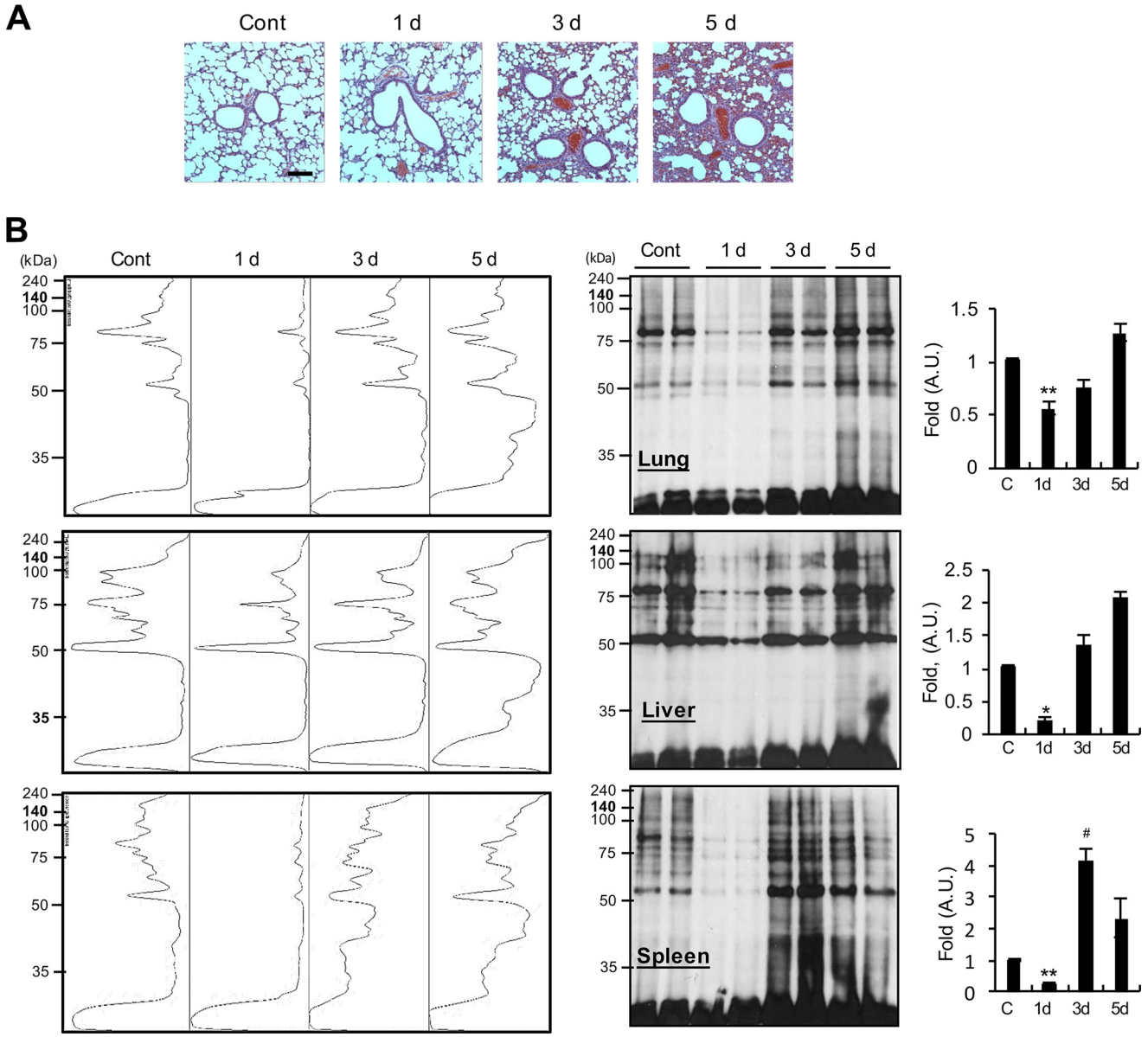

Figure 6. Time course histological changes in pulmonary tissue and protein *O*-GlcNAcylation changes in lung, liver, and spleen in response to LPS. Mice were intraperitoneally injected with PBS or LPS (5 mg/kg). *A,* lung injury was assessed via H&E staining and histological examination on days 1, 3, and 5. *Scale bar*, 500 μm. *B,* total lysates from lung, liver, and spleen were prepared and *O*-GlcNAcylation analyzed via Western blotting using the anti-*O*-GlcNAc CTD110.6 antibody. Representative Western blot analysis and quantification in a spectral mode of *O*-GlcNAcylation are shown. Blots are representative of three independent experiments. All values are mean ± S.E. *Asterisks* denote significantly decreased from the untreated control (*, $p < 0.05$; **, $p < 0.01$); *hash mark* (#) indicates significantly increased from the untreated control ($p < 0.05$).

O-GlcNAcylation, whereas the LPS + GlcN group displayed increased *O*-GlcNAcylation up to the control level in Western blotting experiments (Fig. 9*A*, *left panel*). Similarly, labeling of *O*-GlcNAc with galactosyltransferase using [^{3}H]galactose as a substrate showed that LPS reduced *O*-GlcNAcylation, which was increased by GlcN in RAW264.7 cells (Fig. 9*A*, *right panel*). We compared the cell type–specific changes of *O*-GlcNAcylation, OGT, and OGA levels in response to LPS and/or GlcN using RAW264.7 (macrophage), HepG2 (hepatocyte), NIH-3T3 (fibroblast), and HEK-293 cells (epithelial cells); *O*-GlcNAcylation was regulated by LPS and/or GlcN in RAW264.7 and HepG2 cells but not in NIH-3T3 and HEK-293 cells (Fig. S4). To further investigate the potential correlation between *O*-GlcNAc reduction by LPS and inflammatory gene expression, we examined the effects of PUGNAc, a specific inhibitor of OGA, on LPS-induced iNOS expression in RAW264.7 cells. PUGNAc triggered a significant increase in *O*-GlcNAcylation in both the presence and absence of LPS and a corresponding dose-dependent decrease in LPS-induced iNOS expression (Fig. 9*B*). The inhibitory effect of PUGNAc on LPS-induced inflammatory genes was further confirmed by experiments showing PUGNAc-mediated suppression of *iNos*, *Cox-2*, and *Il-1*β mRNA expression in RAW264.7 cells (Fig. 9*C*). We then measured secreted IL-1β in culture medium of RAW264.7 cells by ELISA and Western blotting. LPS increased the accumulation of this cytokine but PUGNAc did not significantly alter LPS-induced IL-1β accumulation at 24 h (Fig. S5). Next, the effects of pharmacological OGA inhibitors on LPS-

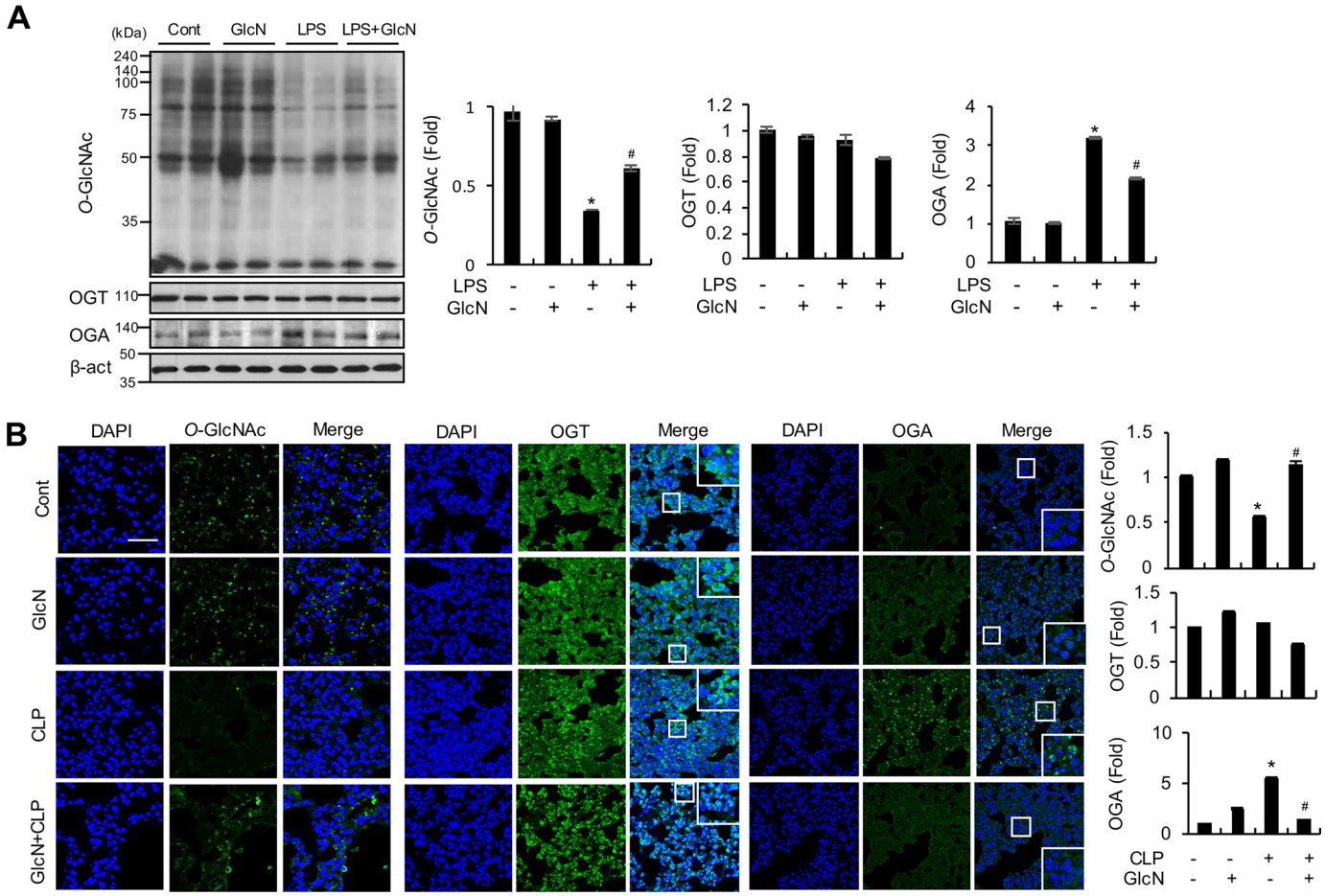

Figure 7. Changes in *O*-GlcNAcylation, OGT, and OGA levels in mouse lung tissue in response to LPS and/or GlcN. *A,* mice were intraperitoneally injected with LPS (5 mg/kg) and/or GlcN (200 mg/kg), and lungs were isolated at 24 h. Total lysates from lung tissue were subjected to Western blot analysis using CTD110.6 antibody. A representative blot is shown. Relative densitometric intensities of *O*-GlcNAc, OGA, and OGT were quantitatively measured by normalizing to β-ACTIN levels. *B,* mice underwent sham (*Cont*) or CLP operation on day 0. At 1 h before surgery, mice were subjected to intraperitoneal injection with GlcN (200 mg/kg) or PBS. Representative confocal immunofluorescence staining images of *O*-GlcNAc, OGT, and OGA were shown. Nuclei were counterstained with DAPI for visualization in lung tissue and positive staining for *O*-GlcNAc, OGT, and OGA (MGEA5) quantitatively measured and graphed. *Scale bar*, 500 μm. Blots and fluorescent images are representative of three independent experiments. All values are presented as mean ± S.E. *Asterisk* denotes significantly increased from the untreated control ($p < 0.05$); *hash mark* (#) indicates significantly decreased from LPS-stimulated conditions ($p < 0.05$).

induced inflammation were examined in a zebrafish sepsis model. LPS triggered an increase in *inos*, *cox-2*, *il-6*, *il-1β*, *ifn-α*, *ifn-β*, *ifn-γ*, and *tnf-α* mRNA levels in the visceral tissue of adult zebrafish at 24 h. Pretreatment with the OGA inhibitors, PUGNAc and Thiamet-G, significantly suppressed LPS-induced proinflammatory gene expression, except ifn-β (Fig. 9*D*).

OGA knockdown increases LPS-induced iNOS/NO in RAW264.7 cells

To ascertain the role of OGA in LPS-induced inflammation, RAW264.7 cells were transfected with shRNA specifically targeting *Oga* and single clones stably expressing *Oga*-shRNA were selected. Our results confirmed a dramatic decrease in the OGA protein level in two independent clones, compared with the control shRNA clone (Fig. 10, *A* and *B*). *Oga* knockdown clones displayed increased *O*-GlcNAcylation in control as well as LPS and/or GlcN treatment conditions. Furthermore, *Oga* knockdown led to increased iNOS expression and nitrite production in response to LPS (Fig. 10, *A–C*). Interestingly, OGT expression was decreased in *Oga* knockdown cells with or without GlcN (Fig. 10, *A* and *B*) and elevated in the presence of LPS, which was abolished upon GlcN pretreatment.

Discussion

Despite impressive advances in biomedical research, limited breakthroughs have been made in the treatment of sepsis, primarily due to the intricate and heterogenic nature of systemic immune responses. Therefore, the development of appropriate animal models and optimization of study conditions is essential to uncover the biological mechanisms underlying this condition. Lethal septic shock is required to examine survival following sepsis, whereas sublethal septic stimulation should be applied to determine cell and tissue or immune responses after sepsis. In the current study, the CLP mouse model was employed to evaluate the survival effects of GlcN, because controlling the puncture count was an easy and reliable method to obtain consistent survival rates and establish its protective effects. In our experimental septic animal model, CLP challenge resulted in an 11% survival rate within 10 days. Administration of GlcN not only extended the survival time but also improved

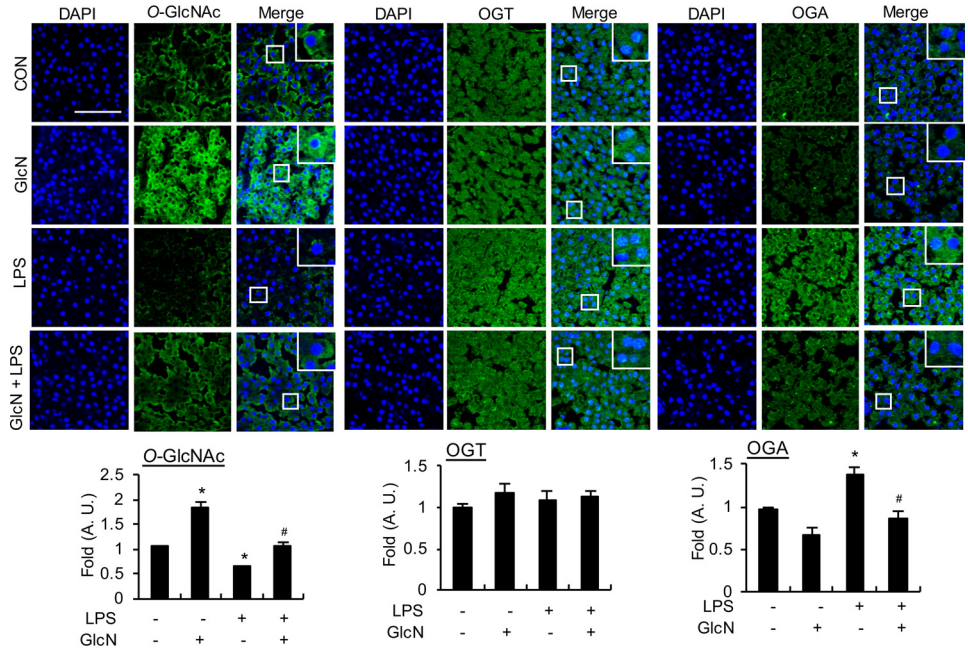

Figure 8. Changes in *O*-GlcNAcylation, OGT, and OGA levels in visceral tissue of zebrafish in response to LPS and/or GlcN. Adult zebrafish were incubated with GlcN (1 g/liter in maintained water) for 12 h before abdominal GlcN (200 μg/g) injection and subsequently stimulated with LPS (100 μg/g). Visceral tissues were separated at 24 h. Representative confocal immunofluorescence staining images of *O*-GlcNAc, OGT, and OGA are shown. Nuclei were counterstained with DAPI for visualization in tissue and positive staining for *O*-GlcNAc, OGT, and OGA quantitatively measured and graphed. Fluorescent images are representative of three independent experiments. All values are mean ± S.E. *Asterisk* denotes significantly increased from the untreated control ($p < 0.05$); *hash mark* (#) indicates significantly decreased from LPS-stimulated conditions ($p < 0.05$). *Scale bar*, 50 μm.

the survival rate to 55%. Lethality was significantly more variable in the LPS endotoxemia model in mouse, probably due to the flexible and variable survival responses of individual animals after LPS injection. The LPS animal model was considered appropriate to study the sublethal toxic effects of sepsis, because LPS induced consistent inflammatory responses in mouse. Therefore, in the present study, we employed the CLP model to examine the effect of GlcN on lethality, whereas the LPS model for moderate sepsis was applied to examine the inhibitory effect of GlcN on lung and systemic inflammation in mice. We additionally used the zebrafish system to investigate LPS-induced inflammatory responses in visceral tissue of adult zebrafish. The advantages of using zebrafish for inflammatory research are numerous, including its small size, easy handling, relatively small amount of drug used, and ease of drug administration (either injection or treatment via dissolving in water), as well as its highly developed vertebrate immune system. Although LPS was able to induce strong inflammatory response in the intestine of adult zebrafish, treatment did not induce death up to a concentration of 2 mg/g body weight. Previous reports have demonstrated that the LPS receptor cluster with CXCR4 in zebrafish is tightly controlled to avoid excess inflammation (28). Furthermore, because fish live in water where they are potentially in intimate contact with higher levels of microorganisms, compared with mammals, inflammation and sepsis should be more tolerable in fish. Although we failed to determine the effects of GlcN on septic death, our results indicate that a sublethal endotoxemic model of zebrafish presents a stable and consistent system to investigate the immune regulatory mechanisms of GlcN as well as screening anti-inflammatory molecules in the future.

Early organ damage in sepsis is caused by excess or severe inflammation. The lung is particularly affected by sepsis and ALI can develop as a result, which contributes to the high mortality rate (29). Data from the current study have revealed a strong anti-inflammatory effect of GlcN in a sepsis model by attenuating pulmonary edema, neutrophil infiltration, nitrite production, and inflammatory cytokine production, as well as M1 polarization. GlcN is reported to attenuate LPS-induced lung inflammation in rats (30). The earlier study used intratracheal instillation of LPS to elicit local lung inflammation in rat and anti-inflammatory effects of GlcN in response to the cytokine mixture are examined using the rat alveolar cell line, L2. However, the effects of GlcN on septic lethality, systemic inflammation, and septic lung injury have never been examined to date. The CLP and intraperitoneal LPS injection models used in the current study usually generate a systemic inflammatory response involving a more intact immune condition, with interactions between the lung and whole body. Our findings disclose for the first time that GlcN protects against LPS- and CLP-induced endotoxemia and sepsis via broad-spectrum anti-inflammatory effects.

Septic response is characterized by increased levels of inflammatory cytokines, such as COX-2, TNF-α, IL-1β, and IL-6, and NO. The significance of MAPKs and NF-κB in endotoxic shock has been established. Activation of MAPK and NF-κB signaling increases the production of proinflammatory cytokines (31) and inhibition of MAPK significantly reduces mortality associated with sepsis in rats with endotoxic shock (31). We and other groups have shown that GlcN exerts an anti-inflammatory effect via suppression of MAPK and/or NF-κB signaling pathways (23, 32–35). In our experiment,

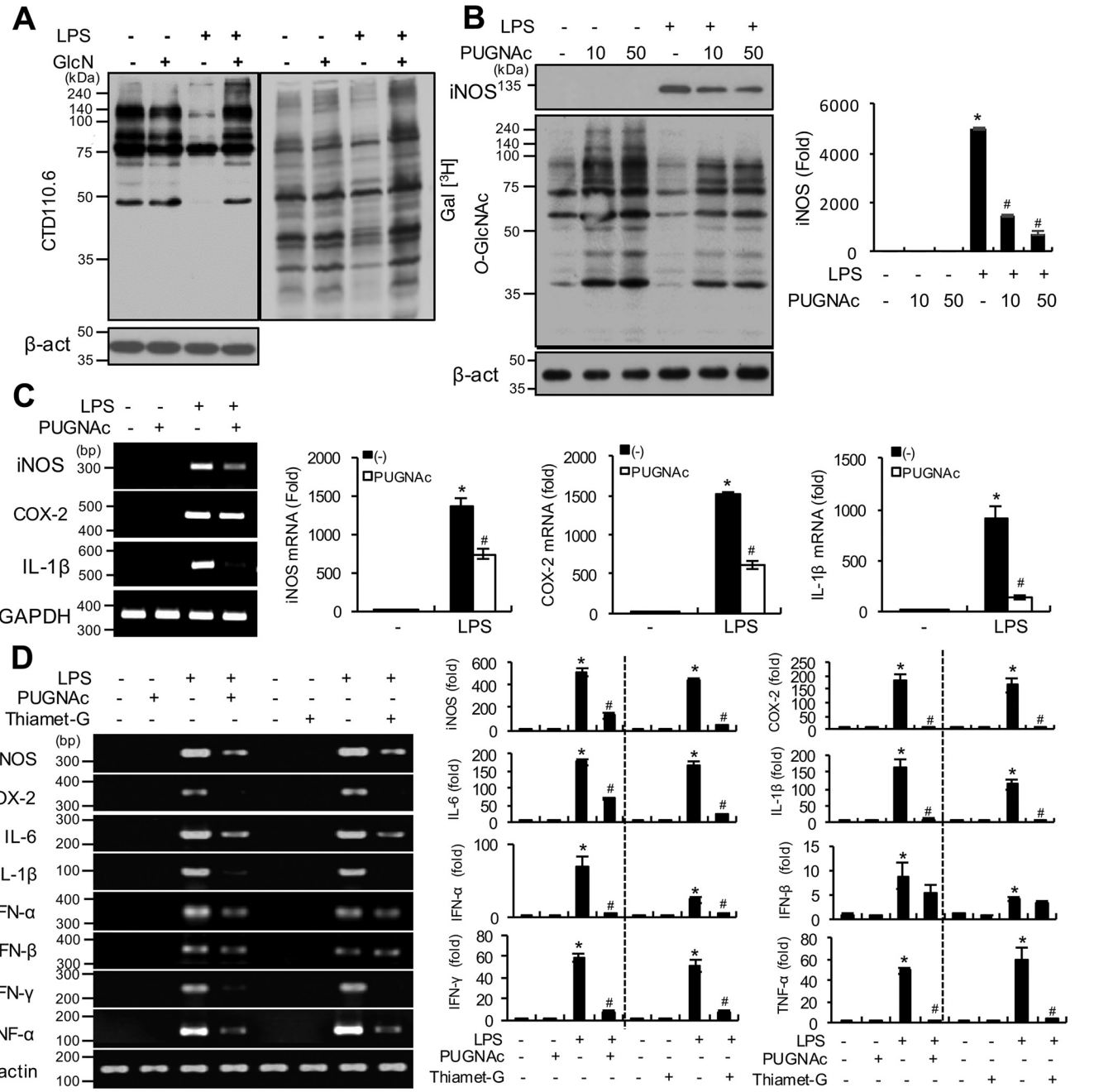

Figure 9. *O*-GlcNAcylation changes in response to LPS and/or GlcN in RAW264.7 cells and effects of OGA inhibitors on LPS-induced inflammatory gene induction. *A,* RAW 264.7 cells were pre-treated with GlcN (5 mM) for 2 h, followed by stimulation with LPS (100 ng/ml) for 24 h. Whole cell lysates were prepared and subjected to Western blotting for *O*-GlcNAcylation using the CTD110.6 antibody (*left panel*) or galactosyltransferase-labeled using [^{3}H]UDP-galactose as a substrate and exposed to X-ray film for autoradiography (*right panel*). *B,* RAW 264.7 cells were pre-treated with PUGNAc (10 or 50 μM) for 2 h and subsequently stimulated with LPS (100 ng/ml) for 24 h. *O*-GlcNAcylation levels of total cell lysates were measured via Western blotting using the CTD110.6 antibody. The graph represents relative densitometric intensities that were quantitatively measured and normalized to β-ACTIN levels. *C,* RAW 264.7 cells were stimulated with LPS (100 ng/ml) with or without PUGNAc (0.5 mM) for 24 h. Expression of *iNos*, *Cox-2*, and *Il-1β* mRNA were determined by RT-PCR (*left panel*) and quantitatively assessed using real-time PCR (*right graphs*). *Gapdh* was determined as the loading control. Results are representative of three independent experiments. All values are mean ± S.E. *D,* adult zebrafish were treated with PUGNAc (50 μg/g) or Thiamet-G (20 μg/g) for 2 h and injected with LPS (100 μg/g). Visceral tissues were isolated at 24 h and mRNA expression of *inos*, *cox-2*, *il-6*, *il-1β*, *ifn-α*, *ifn-β*, *ifn-γ*, and *tnf-α* determined using PCR (*left panel*) and quantitative real-time PCR (*right graphs*). Results are representative of three independent experiments. All values are mean ± S.E. *Asterisk* denotes significantly increased from the untreated control ($p < 0.05$); *hash mark* (#) indicates significantly decreased from LPS-stimulated conditions ($p < 0.05$).

GlcN inhibited phosphorylation of JNK, P38 MAPK, ERK1/2, IκB, and P65 in lungs of LPS septic mice. These findings suggest that GlcN can improve lung and systemic inflammation via inhibition of the MAPK and NF-κB pathway to suppress production of NO and other inflammatory mediators in a sepsis model.

Macrophages demonstrate characteristics of diversity and plasticity leading to the acquisition of various phenotypes. Based on phenotype, macrophages are classified into classically activated (M1) and alternatively activated (M2) depending on gene expression profiles. The proportion or degree of differentiation of macrophages is important in the initiation, progres-

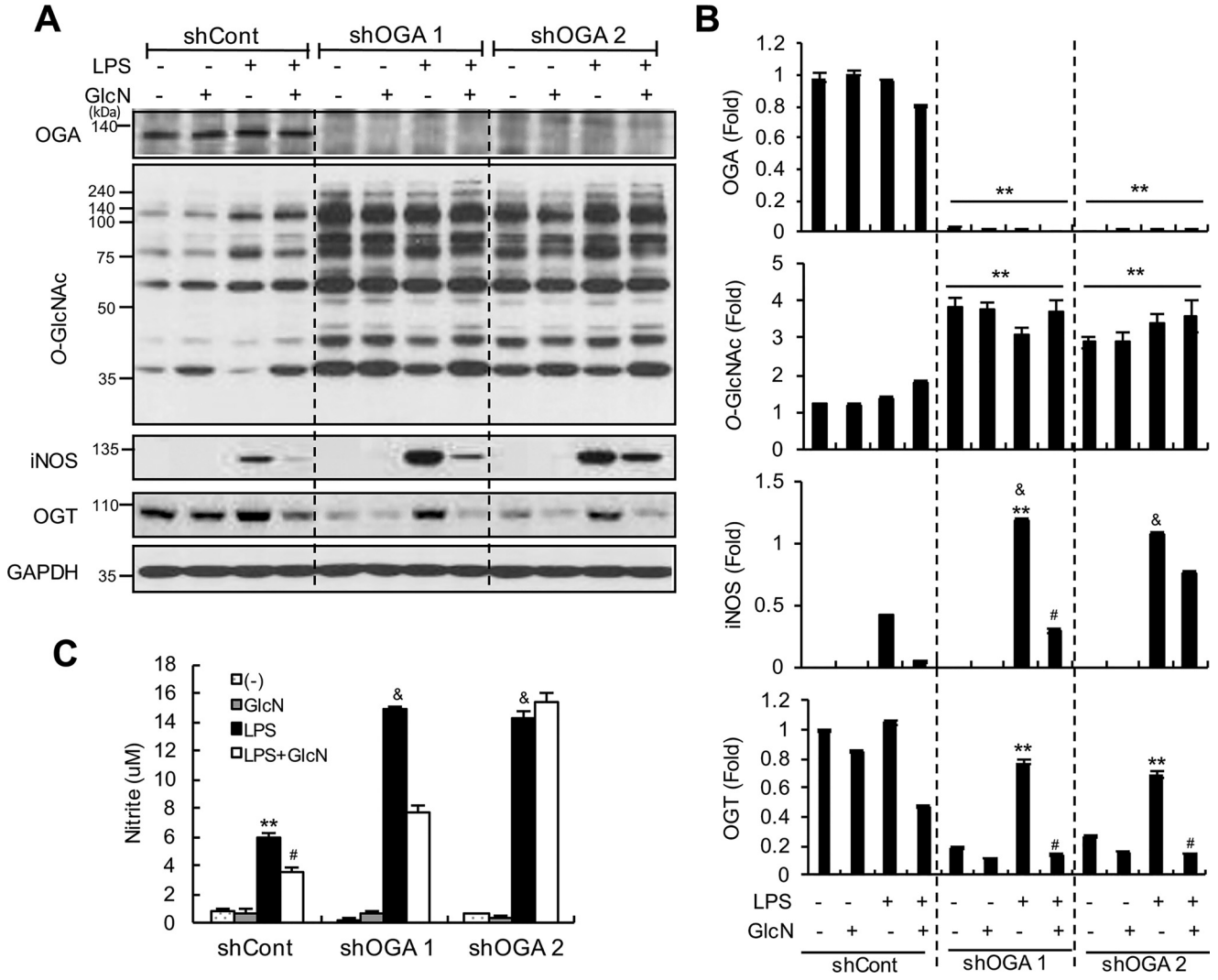

Figure 10. Effect of *Oga* knockdown on LPS-mediated iNOS/NO induction. *Oga* knockdown cells were generated via stable transfection of shCont, sh*Oga*1, and sh*Oga*2. Control and *Oga* knockdown cells were stimulated with LPS (100 ng/ml) with or without 5 mM GlcN for 24 h. Whole cell lysates were prepared and the expression levels of OGA, *O*-GlcNAc, iNOS, and OGT were measured via Western blotting using anti-MGEA5, CTD110.6, anti-iNOS, and anti-OGT antibodies, respectively (*A*). Relative densitometric intensities were quantitatively measured and normalized to GAPDH levels (*B*). Nitrite levels in cell culture medium were measured with the Griess assay (*C*). Blots are representative of three independent experiments. All values are presented as mean ± S.E. *Asterisks* denote significantly increased from the untreated control (*, $p < 0.05$; **, $p < 0.01$); *hash mark* (#) indicates significantly decreased from LPS-stimulated conditions ($p < 0.05$); &, indicates significantly increased from shCont LPS-stimulated conditions ($p < 0.05$).

sion, and termination of numerous inflammatory diseases. In general, sepsis is associated with increased monocyte expression of M1 markers and decreased expression of M2 markers in mice (36). One suggested mechanism for the beneficial effects of GlcN on sepsis or inflammation is that increased hexosamine biosynthetic pathway flux by GlcN suppresses the M1-like phenotype. However, as mRNA expression is not always correlated with protein levels or enzymatic activity, M1 and M2 phenotype markers should be extensively analyzed in the future to draw definite conclusions regarding the role of GlcN in LPS-induced macrophage polarization.

To investigate the molecular mechanisms underlying the anti-inflammatory effects of GlcN on sepsis, we examined the changes in *O*-GlcNAcylation in proteins from lung tissues of mice in response to LPS with or without GlcN pretreatment. LPS suppressed *O*-GlcNAcylation of nucleocytoplasmic proteins of lung tissue on day 1, which was subsequently recovered on day 3, suggesting a critical role of this modification in the control of inflammatory reactions as well as subsequent recovery responses. Our observation of GlcN-mediated protection against reduction of LPS-induced *O*-GlcNAcylation further supported the importance of acute *O*-GlcNAcylation changes induced by septic shock in modulating inflammatory responses. Initial acute elevation (1–4 h after ischemia) and a subsequent marked decline in protein *O*-GlcNAcylation has been previously reported during permanent cerebral ischemia in a middle cerebral artery occlusion mouse model (37). However, our investigation of acute *O*-GlcNAcylation changes after 10 min and 6 h of LPS treatment was not significantly altered in lung tissue of mice. In association with the *O*-GlcNAcylation change, we showed that down-regulation of *O*-GlcNAcylation in LPS-induced lung tissues of mice and visceral tissue of zebrafish is accompanied by an increase in OGA, with no concomitant changes in the OGT level. Although a role of OGT-

mediated *O*-GlcNAcylation of NF-κB in activating acute pancreatitis has been demonstrated (25), the potential function of OGA in regulation of inflammation is yet to be examined. Accordingly, we hypothesized that up-regulation of OGA and subsequent *O*-GlcNAc reduction present critical tissue responses to septic inflammation. Consistent with this theory, treatment with OGA inhibitors suppressed the inflammatory response to LPS, both *in vitro* and *in vivo*. However, in contrast to our prediction that the inflammatory response is inhibited by down-regulation of OGA protein, shRNA-mediated knockdown of *Oga* further increased LPS-induced inflammation in RAW264.7 cells. One possible explanation for this discrepancy is that, whereas OGA plays an important role, it is not the only regulator, and interactions with other factors or compensatory regulation of OGA down-regulation may further contribute to regulating the overall inflammatory response. One of the results supporting this hypothesis is that *Oga* knockdown led to a concomitant decrease in OGT protein expression. Therefore, unlike pharmacological inhibition, changes in the OGA protein levels are compensated through inducing changes in the amounts of other related proteins. Another possible mechanism for the opposing effects of *Oga* knockdown and inhibition may hinge on the presence of a domain with intrinsic histone acetyltransferase (HAT) activity in OGA (38). Therefore, *Oga* knockdown may modulate iNOS expression via a reduction in its HAT activity rather than through a change in its *O*-GlcNAcase activity. However, we believe that this is unlikely because we previously demonstrated that increased HAT activity (triggered by overexpression of P300/CBP) increases LPS-induced iNOS expression in RAW264.7 cells (39) indicating that HAT can act as a positive regulator of *iNos* gene induction. Overall, the *Oga* knockdown-induced changes in OGT and/or *O*-GlcNAcylation and subsequent inflammatory regulation are likely to be complicated by interactions among enzyme levels, enzyme activities, and the functions of OGA and OGT beyond *O*-GlcNAcylation.

In conclusion, GlcN reduces the lethality of septic shock and exerts protective effects against septic lung injury through suppression of inflammation. Our findings further suggest that dynamic changes in the *O*-GlcNAc level in response to LPS are possibly associated with regulation of OGA expression. Although it remains unclear why pharmacological inhibition and down-regulation of OGA protein generated conflicting results with regard to expression of iNOS in response to LPS, this intriguing finding highlights the dynamic changes in OGA expression and *O*-GlcNAcylation during LPS-induced inflammation and supports the potential utility of OGA as a therapeutic target in endotoxemia and septic lung injury.

Materials and methods

Reagents

PUGNAc was from Toronto Research Chemicals (Toronto, Canada) and Thiamet-G was from Sigma. LPS from *Escherichia coli* O111:B4 was from Sigma.

Animal conditioning

Male Balb/c, 6–7 weeks of age and weighing 20–25 g, were purchased from SAMTACO (Osan, South Korea). Mice were individually housed under 12-h light/dark cycles at 22 ± 2 °C. All animal experiments were approved by the Institutional Animal Care and Use Committee of Inha University in Incheon (agreement number INHA 1160614-101).

Zebrafish (*D. rerio*) was obtained from the Daesangline aquarium (Seoul, South Korea) and maintained at 27.0 ± 1.0 °C on a 14-h light/10-h dark cycle in accordance to guidelines. We used ~2.5– cm long adult zebrafish for experiments. Tap water passed through a multistage filtration system equipped with a sediment filter, a post-carbon filter, and a fluorescent UV light-sterilizing filter supplied to the aquarium containers for the fish (Zebrafish AutoSystem, Genomic Design, Seoul, South Korea). Water in the containers was aerated continuously and maintained at pH 6.5–7.5. The zebrafish were fed twice a day with flake food (TetraBits, Luzerne, Singapore) and had access to live brine shrimp *ad libitum*.

Sepsis animal model

An experimental CLP sepsis mouse model was established as described previously (40). In brief, Balb/c mice were anesthetized via inhalation of isoflurane, after which a stump was punctured once with a 22-gauge needle to extrude a small amount of stool. The cecum was placed back into its normal intraabdominal position and the abdomen closed. Next, 0.3 ml of saline was administered subcutaneously (intraperitoneally) for fluid resuscitation. Sham-operated control mice underwent the same surgical procedures without puncture or ligation. Mice were returned to cages and provided food and water *ad libitum*. The mortality rate was monitored every day for 12 days. For generation of the LPS-induced mouse sepsis model, male Balb/c mice were injected intraperitoneally with LPS (5 mg/kg of body weight) or control PBS. To examine the effects of GlcN, mice were provided a solution of 5% (w/v) D-(+)-glucosamine hydrochloride dissolved in drinking water adjusted to 7 h before LPS injection. GlcN dissolved in PBS (pH 7.4) was administered intraperitoneally at a concentration of 200 mg/kg body weight 1 h before LPS injection. The zebrafish LPS sepsis model was generated by microinjecting LPS (100 μg/g of body weight) in PBS or PBS only for the control group after anesthetization with 0.03% MS-222 and maintained in normal water. For GlcN groups, zebrafish were maintained in GlcN (1 g/liter) containing water for 12 h and injected intraperitoneally with GlcN (200 μg/g) for 2 h followed by LPS administration. PUGNAc (50 μg/g) or Thiamet-G (20 μg/g) were intraperitoneally injected 2 h prior to LPS administration.

Lung wet-to-dry ratio

The lung wet-to-dry ratio was determined as described previously (41). The right lung was separated, weighed (wet weight), and then dried overnight in a 60 °C oven (dry weight). Wet/dry weight ratio was calculated by dividing the wet weight by the dry weight.

Histological examination and immunohistochemistry

The right lung tissues were excised, washed with PBS, fixed with 4% formalin buffer (4% formaldehyde, 30 mM NaH_2PO_4, 45 mM Na_2HPO_4), and paraffin-embedded. For histological examination, 4-μm sections of formalin-fixed paraffin-embed-

ded lung tissues were cut, placed on glass slides, deparaffinized with xylene, and rehydrated in 30–100% ethanol. Sections were boiled in retrieval buffer (10 mM citrate buffer, pH 6.0) using a microwave for 5 min and stained with H&E for histopathological examination. For immunofluorescence staining, sections were incubated in blocking buffer (10% normal goat serum in PBS, 0.1% Triton X-100) for 1 h at room temperature, followed by incubation with anti-iNOS antibody (BD Transduction, Lexington, KY, 610107) overnight at 4 °C. After washing, sections were incubated with secondary antibody for 1 h at room temperature, treated with the avidin-biotin-peroxidase complex for 15 min, and stained with diaminobenzidine for 5 min. Stained sections were analyzed under a light microscope (Carl Zeiss, Jena, Germany).

Immunofluorescence staining

Paraffin-embedded sections of mouse lung tissues were deparaffinized and rehydrated as specified above. Adult zebrafish were anesthetized with 0.03% MS-222, and the intestine removed and fixed in 4% paraformaldehyde. The tissue was cut into 10-μm cross-plane sections with a cryostat (CM1800; Leica, Wetzlar, Germany). Sections were mounted onto coated slides (Matsunami Glass Ind., Ltd., Osaka, Japan) and stored at −20 °C until further use. For immunofluorescence staining, slides (both mouse and zebrafish) were incubated with blocking buffer and probed with anti-*O*-GlcNAc CTD110.6 (Covance, Berkeley, CA, MMS-248R), anti-OGT (Santa Cruz, sc-32921), anti-OGA (Proteintech, 14711-1-AP), anti-LY6G (R&D Systems, MAB1037-100), Ser-32-specific anti-phospho-IκBα (Santa Cruz, sc-101713) or Ser-536-specific anti-phospho-P65 (Abcam, ab86299) antibodies. Next, slides were incubated with Alexa Fluor® 488 (green)-conjugated secondary antibodies (Molecular Probes, Eugene, OR, A11008). DAPI staining for identification of nuclei was performed for 5 min. Slides were examined under the LSM 510 META (Carl Zeiss) confocal microscope and analyzed using ZEN Light Edition software.

Determination of cytokines by ELISA

Whole blood was collected by cardiac puncture into syringes and samples were tubed and placed at room temperature for 30 min. After centrifuging (6,000 rpm, 15 min, room temperature), plasma obtained and supernatant were immediately frozen in liquid nitrogen (LN_2) and stored at −70 °C until further analysis. The levels of IL-1β, IL-6, or TNF-α in plasma or culture medium were measured using ELISA kits (R&D Systems). Results were determined spectrophotometrically using a microphage reader.

Measurement of nitric oxide

Nitric oxide quantified colorimetrically measurements of nitrite/nitrate levels in serum and cell culture medium by the Griess reagent assay. Fifty microliters of samples were mixed with an equal volume of Griess reagent (1% sulfanilamide, 0.1% naphthylenediamine, and 5% phosphoric acid). Absorbance was measured at 540 nm using a microreader, and nitrite concentration was assessed against a sodium nitrite standard curve (0–100 μM).

Western blotting

Lung tissue was homogenated in lysis buffer (150 mM NaCl, 300 mM sucrose, 1 mM EDTA, protease and phosphatase inhibitors, and 20 μM streptozotocin (pH 8.0)) and centrifuged for 20 min at 13,200 rpm. Cells were lysed in Nonidet P-40 lysis buffer (150 mM NaCl, 50 mM Tris-HCl (pH 8.0), 0.5% Nonidet P-40 and containing protease and phosphatase inhibitors). 20–40 μg of protein samples were separated by SDS-PAGE, transferred to Amersham Biosciences™ Protran™ nitrocellulose membrane (GE Healthcare Life Science, Germany) and incubated with 5% skim milk or 5% BSA blocking buffer at room temperature. Primary antibodies against anti-*p*-AKT (Ser-473), anti-AKT, and GAPDH (Cell Signaling Technology, Danvers, MA, 9271, 9272, and 2118), anti-*p*-JNK (Invitrogen, 44682G), anti-*p*-P38, anti-JNK, and anti-ERK (Cell Signaling Technology, 4511, 9252, and 4695), anti-*O*-GlcNAc CTD110.6 (Covance, Berkeley, CA, MMS-248R), anti-MGEA5 (Proteintech, 14711-1-AP), anti-iNOS (BD Transduction, 610107), anti-OGT, anti-P65, anti-c-REL, anti-P50, anti-IκBα, Ser-32–specific anti-*p*-IκBα, anti-HDAC1, anti-β-ACTIN, anti-*p*-ERK, and anti-P38 (Santa Cruz, sc-32921, sc-372, sc-71, sc-114, sc-371, sc-101713, sc-6298, sc-47778, sc-7383, and sc-535), and anti-α-TUBULIN (Calbiochem Merck KGaA, Darmstadt, Germany, ABT-170) were probed overnight at 4 °C, washed with TBST, incubated with horseradish peroxidase-conjugated secondary antibodies and detected by the Enhanced Chemiluminescence (ECL) detection system (Promega Corp.). Densitometric quantification of protein bands were detected using ImageJ (NIH).

Bone marrow cell isolation

Bone marrow-derived mononuclear cells were isolated from the tibia and femur of mice by flushing with 20 ml of PBS through a 26-gauge needle. After centrifugation at room temperature for 5 min, cells were immediately lysed with TRIzol™.

Reverse transcription-PCR

Total RNAs from cells or tissues were extracted with TRIzol™ (Invitrogen) and then 10 μg of RNA samples were reverse-transcribed into cDNA using GoScript™ reverse transcriptase (Promega) following the manufacturer's instruction. PCR was performed using specific primers of mouse *Gapdh*, forward, 5′-TCATTGACCTCAACTACAGGT-3′, reverse, 5′-CTAAGCAGTTGGTGGTGCAG-3; *iNos*, forward, 5′-GCATCCCAAGTACGAGTGGT-3, reverse, 5′-CCATGATGGTCACATTCTGC-3; *Cox-2*, forward, 5′-GCTGTACAAGCAGTGGCAAA-3, reverse, 5′-GTCTGGAGTGGGAGGCACT-3; *Il-6*, forward, 5′-CCGGAGAGGAGACTTCACAG-3, reverse, 5′-TGGTCTTGGTCCTTAGCCAC-3; *Il-1β*, forward, 5′-GGAGAAGCTGTGGCAGCTA-3, reverse, 5′-GCTGATGTACCAGTTGGGGA-3; *Tnf-α*, forward, 5′-GACCCTCACACTCAGATCAT-3, reverse, 5′-TTGAAGAGAACCTGGGAGTA-3; *Mcp-1*, forward, 5′-GTCCCTGTCATGCTTCTGGG-3′, reverse, 5′-GAAGACCTTAGGGCAGATGCAG-3′; *Mmr*, 5′-AATGCCACTGCCATGCCTAC-3′, reverse, 5′-CACCAGGATAGCCTTTCCCC-3; *Mgl-1*, 5′-CCTGCTGTTGGTGGTCGTCT-3′, reverse, 5′-CAGGGCCTTCAAGTCCTTCC-3′. Specific primers for zebrafish, *β-actin*, forward, 5′-GTGCCC-

ATCTACGAGGGTTA-3′, reverse, 5′-TCTCAGCTGTGGT-GGTGAAG-3; *inosa*, forward, 5′-CTCCCAGATGCCACTC-CTGA-3′, reverse, 5′-GAACCTCCAAGAAGGTGGGC-3′; *cox-2*, forward, 5′-AATTTGCTGTGGGCCATGAG-3′; reverse, 5′-AAGTTGTCCGGCAACAGTGG-3′; *tnf-α*, forward, 5′- GCG-CTTTTCTGAATCCTAC-3′; reverse, 5′-TGCCCAGTCTG-TCTCCTTCT-3′; *il-1β*, forward, 5′-GCTGGAGATCCAAA-CGGATA-3′, reverse, 5′- ATACGCGGTGCTGATAAACC-3′; *il-6*, forward, 5′-ACATGACGGCATTTGAAGGG-3′; reverse, 5′-TATGGCCTCCAGCAGTCGTT-3′; *ifn-α*, forward, 5′-GGTGGAATATCTGCAGGTTC-3′; reverse, 5′-GC-TTGAAGCAATGACACCA-3′; *ifn-β*, forward, 5′-CTCCTC-TCCTCAAACCTTCA-3′; reverse, 5′-TCTTTCCCTCTTTT-CCTCCT-3′; *ifn-γ*, forward, 5′- CATGCAGAATGACAGCG-TGG-3′; reverse, 5′-TTGATGCTTTAGCCTGCCGT-3′. The PCR products were separated by 1% agarose gel electrophoresis. Quantitative real-time PCR was performed by incubating cDNAs in SYBR Green Real-time PCR master Mix (TOYOBO, Osaka, Japan) with normalization to GAPDH levels.

Cell culture

RAW264.7 murine macrophage cells were purchased from the Korean Cell Line Bank. Cells were maintained in Dulbecco's modified Eagle's medium (Hyclone, Logan, UT) supplemented with 5% FBS (ATCC, Manassas, VA), 1% streptomycin and penicillin (Hyclone) at 37 °C in 5% CO_2 in a humidified atmosphere incubator.

Bone marrow cell isolation and macrophage polarization

BMDM cells were isolated from the tibia and femur of mice by flushing with 20 ml of PBS through a 26-gauge needle. Cells were harvested by centrifugation at room temperature for 5 min and were cultured in the RPMI containing 10% FBS and macrophage–colony-stimulating factor (20 ng/ml). On day 7, cells were harvested and plated in 24-well plate. Cells were pretreated with GlcN (5 mM) and then stimulated with IL-4 (20 ng/ml) or LPS (1 μg/ml) for 24 h.

Generation of Oga knockdown cells

Expression vectors encoding shRNAs targeting *Oga* driven by the U6 promoter containing a puromycin-resistant gene were purchased from Sigma (MISSION® shRNA). RAW264.7 cells were stably transfected using Lipofectamine™ and PLUS™ reagent (Invitrogen) and puromycin-resistant cells were selected by culturing in 1 μg/ml of puromycin-containing medium. In total, 12 independent clones were selected and validated for efficacy of knockdown via PCR and Western blotting in RAW264.7 cells.

Galactosyltransferase assay

O-GlcNAcylated proteins were labeled with galactosyltransferase using its radiolabeled substrate (UDP-[^{3}H]galactose) as described previously (23). Protein lysates were mixed with labeling buffer (5 mM $MnCl_2$, 10 mM galactose, 50 mM HEPES, pH 7.4) and reactions were initiated by the addition of 2 μCi of UDP-[^{3}H]galactose (American Radiolabeled Chemicals, St. Louis, MO) in 5′-AMP solution (2.5 mM) and 50 milliunits of galactosyltransferase (Sigma). The reaction mixture was incubated at 37 °C for 1 h and the reaction was terminated with the addition of SDS sample buffer. Proteins were separated via SDS-PAGE, intensified with EN^{3}HANCE Fluor (PerkinElmer Life Sciences, Waltham, MA), dried, and exposed to X-ray film.

Statistical analysis

Data are expressed as mean ± S.E. and analyzed for statistical significance using analysis of variance, followed by Scheffe's test for multiple comparisons and paired Student's *t* test for comparing between two groups. A p value < 0.05 was considered significant.

Author contributions—J.-S. H., K.-H. K., J. P., S.-M. K., Y. L., and I.-O. H. investigation; J.-S. H., K.-H. K., and I.-O. H. writing-original draft; J. P., S.-M. K., and Y. L. methodology; H. C. and I.-O. H. supervision; H. C., Y. L., and I.-O. H. project administration; Y. L. validation.

References

1. Fleischmann, C., Scherag, A., Adhikari, N. K., Hartog, C. S., Tsaganos, T., Schlattmann, P., Angus, D. C., Reinhart, K., and International Forum of Acute Care Trialists (2016) Assessment of global incidence and mortality of hospital-treated sepsis: current estimates and limitations. *Am. J. Respir. Crit. Care Med.* **193,** 259–272 CrossRef Medline
2. Hasan, Z., Palani, K., Rahman, M., and Thorlacius, H. (2011) Targeting CD44 expressed on neutrophils inhibits lung damage in abdominal sepsis. *Shock* **35,** 567–572 CrossRef Medline
3. Rubenfeld, G. D., Caldwell, E., Peabody, E., Weaver, J., Martin, D. P., Neff, M., Stern, E. J., and Hudson, L. D. (2005) Incidence and outcomes of acute lung injury. *N. Engl. J. Med.* **353,** 1685–1693 CrossRef Medline
4. Kolaczkowska, E., and Kubes, P. (2013) Neutrophil recruitment and function in health and inflammation. *Nat. Rev. Immunol.* **13,** 159–175 CrossRef Medline
5. Kabir, K., Gelinas, J. P., Chen, M., Chen, D., Zhang, D., Luo, X., Yang, J. H., Carter, D., and Rabinovici, R. (2002) Characterization of a murine model of endotoxin-induced acute lung injury. *Shock* **17,** 300–303 CrossRef Medline
6. Lien, E., Means, T. K., Heine, H., Yoshimura, A., Kusumoto, S., Fukase, K., Fenton, M. J., Oikawa, M., Qureshi, N., Monks, B., Finberg, R. W., Ingalls, R. R., and Golenbock, D. T. (2000) Toll-like receptor 4 imparts ligand-specific recognition of bacterial lipopolysaccharide. *J. Clin. Invest.* **105,** 497–504 CrossRef Medline
7. Sakaguchi, M., Marutani, E., Shin, H. S., Chen, W., Hanaoka, K., Xian, M., and Ichinose, F. (2014) Sodium thiosulfate attenuates acute lung injury in mice. *Anesthesiology* **121,** 1248–1257 CrossRef Medline
8. Wang, N., Liang, H., and Zen, K. (2014) Molecular mechanisms that influence the macrophage m1-m2 polarization balance. *Front. Immunol.* **5,** 614 Medline
9. Wong, J. M., and Billiar, T. R. (1995) Regulation and function of inducible nitric oxide synthase during sepsis and acute inflammation. *Adv. Pharmacol.* **34,** 155–170 CrossRef Medline
10. Fan, J., Ye, R. D., and Malik, A. B. (2001) Transcriptional mechanisms of acute lung injury. *Am. J. Physiol. Lung Cell Mol. Physiol.* **281,** L1037–L1050 CrossRef Medline
11. D'Alessio, F. R., Tsushima, K., Aggarwal, N. R., Mock, J. R., Eto, Y., Garibaldi, B. T., Files, D. C., Avalos, C. R., Rodriguez, J. V., Waickman, A. T., Reddy, S. P., Pearse, D. B., Sidhaye, V. K., Hassoun, P. M., Crow, M. T., and King, L. S. (2012) Resolution of experimental lung injury by monocyte-derived inducible nitric oxide synthase. *J. Immunol.* **189,** 2234–2245 CrossRef Medline
12. Aderem, A., and Ulevitch, R. J. (2000) Toll-like receptors in the induction of the innate immune response. *Nature* **406,** 782–787 CrossRef Medline
13. Bai, D., Ueno, L., and Vogt, P. K. (2009) Akt-mediated regulation of NFκB and the essentialness of NFκB for the oncogenicity of PI3K and Akt. *Int. J. Cancer* **125,** 2863–2870 CrossRef Medline

14. Poli-de-Figueiredo, L. F., Garrido, A. G., Nakagawa, N., and Sannomiya, P. (2008) Experimental models of sepsis and their clinical relevance. *Shock* **30,** 53–59 CrossRef Medline
15. van der Vaart, M., Spaink, H. P., and Meijer, A. H. (2012) Pathogen recognition and activation of the innate immune response in zebrafish. *Adv. Hematol.* **2012,** 159807 Medline
16. Sunyer, J. O. (2013) Fishing for mammalian paradigms in the teleost immune system. *Nat. Immunol.* **14,** 320–326 CrossRef Medline
17. Stachura, D. L., Svoboda, O., Campbell, C. A., Espín-Palazon, R., Lau, R. P., Zon, L. I., Bartunek, P., and Traver, D. (2013) The zebrafish granulocyte colony-stimulating factors (Gcsfs): 2 paralogous cytokines and their roles in hematopoietic development and maintenance. *Blood* **122,** 3918–3928 CrossRef Medline
18. Lieschke, G. J., and Trede, N. S. (2009) Fish immunology. *Curr. Biol.* **19,** R678–R682 CrossRef Medline
19. Trede, N. S., Langenau, D. M., Traver, D., Look, A. T., and Zon, L. I. (2004) The use of zebrafish to understand immunity. *Immunity* **20,** 367–379 CrossRef Medline
20. Comer, F. I., and Hart, G. W. (2000) *O*-Glycosylation of nuclear and cytosolic proteins: dynamic interplay between *O*-GlcNAc and *O*-phosphate. *J. Biol. Chem.* **275,** 29179–29182 CrossRef Medline
21. Butkinaree, C., Park, K., and Hart, G. W. (2010) *O*-Linked β-*N*-acetylglucosamine (O-GlcNAc): extensive crosstalk with phosphorylation to regulate signaling and transcription in response to nutrients and stress. *Biochim. Biophys. Acta* **1800,** 96–106 CrossRef Medline
22. Hu, P., Shimoji, S., and Hart, G. W. (2010) Site-specific interplay between *O*-GlcNAcylation and phosphorylation in cellular regulation. *FEBS Lett.* **584,** 2526–2538 CrossRef Medline
23. Hwang, J. S., Kwon, M. Y., Kim, K. H., Lee, Y., Lyoo, I. K., Kim, J. E., Oh, E. S., and Han, I. O. (2017) Lipopolysaccharide (LPS)-stimulated iNOS induction is increased by glucosamine under normal glucose conditions but is inhibited by glucosamine under high glucose conditions in macrophage cells. *J. Biol. Chem.* **292,** 1724–1736 CrossRef Medline
24. He, Y., Ma, X., Li, D., and Hao, J. (2017) Thiamet G mediates neuroprotection in experimental stroke by modulating microglia/macrophage polarization and inhibiting NF-κB p65 signaling. *J. Cereb. Blood Flow Metab.* **37,** 2938–2951 CrossRef
25. Zhang, D., Cai, Y., Chen, M., Gao, L., Shen, Y., and Huang, Z. (2015) OGT-mediated *O*-GlcNAcylation promotes NF-κB activation and inflammation in acute pancreatitis. *Inflamm. Res.* **64,** 943–952 CrossRef Medline
26. Hwang, S. Y., Shin, J. H., Hwang, J. S., Kim, S. Y., Shin, J. A., Oh, E. S., Oh, S., Kim, J. B., Lee, J. K., and Han, I. O. (2010) Glucosamine exerts a neuroprotective effect via suppression of inflammation in rat brain ischemia/reperfusion injury. *Glia* **58,** 1881–1892 CrossRef Medline
27. Forn-Cuní, G., Varela, M., Pereiro, P., Novoa, B., and Figueras, A. (2017) Conserved gene regulation during acute inflammation between zebrafish and mammals. *Sci. Rep.* **7,** 41905 CrossRef Medline
28. Novoa, B., Bowman, T. V., Zon, L., and Figueras, A. (2009) LPS response and tolerance in the zebrafish (*Danio rerio*). *Fish Shellfish Immunol.* **26,** 326–331 CrossRef Medline
29. Levy, B. D., and Serhan, C. N. (2014) Resolution of acute inflammation in the lung. *Annu. Rev. Physiol.* **76,** 467–492 CrossRef Medline
30. Chuang, K. H., Peng, Y. C., Chien, H. Y., Lu, M. L., Du, H. I., and Wu, Y. L. (2013) Attenuation of LPS-induced lung inflammation by glucosamine in rats. *Am. J. Respir. Cell Mol. Biol.* **49,** 1110–1119 CrossRef Medline
31. Morales, M. G., Olguín, H., Di Capua, G., Brandan, E., Simon, F., and Cabello-Verrugio, C. (2015) Endotoxin-induced skeletal muscle wasting is prevented by angiotensin-(1–7) through a p38 MAPK-dependent mechanism. *Clin. Sci. (Lond.)* **129,** 461–476 CrossRef Medline
32. Chou, W. Y., Chuang, K. H., Sun, D., Lee, Y. H., Kao, P. H., Lin, Y. Y., Wang, H. W., and Wu, Y. L. (2015) Inhibition of PKC-induced COX-2 and IL-8 expression in human breast cancer cells by glucosamine. *J. Cell. Physiol.* **230,** 2240–2251 CrossRef Medline
33. Zheng, G. M., Yu, C., and Yang, Z. (2012) Puerarin suppresses production of nitric oxide and inducible nitric oxide synthase in lipopolysaccharide-induced N9 microglial cells through regulating MAPK phosphorylation, *O*-GlcNAcylation and NF-κB translocation. *Int. J. Oncol.* **40,** 1610–1618 Medline
34. Tsai, C. Y., Lee, T. S., Kou, Y. R., and Wu, Y. L. (2009) Glucosamine inhibits IL-1β-mediated IL-8 production in prostate cancer cells by MAPK attenuation. *J. Cell. Biochem.* **108,** 489–498 CrossRef Medline
35. Fülöp, N., Zhang, Z., Marchase, R. B., and Chatham, J. C. (2007) Glucosamine cardioprotection in perfused rat hearts associated with increased *O*-linked *N*-acetylglucosamine protein modification and altered p38 activation. *Am. J. Physiol. Heart Circ. Physiol.* **292,** H2227–H2236 CrossRef Medline
36. Sica, A., and Mantovani, A. (2012) Macrophage plasticity and polarization: *in vivo* veritas. *J. Clin. Invest.* **122,** 787–795 CrossRef Medline
37. Gu, J. H., Shi, J., Dai, C. L., Ge, J. B., Zhao, Y., Chen, Y., Yu, Q., Qin, Z. H., Iqbal, K., Liu, F., and Gong, C. X. (2017) *O*-GlcNAcylation reduces ischemia-reperfusion-induced brain injury. *Sci. Rep.* **7,** 10686 CrossRef Medline
38. Toleman, C., Paterson, A. J., Whisenhunt, T. R., and Kudlow, J. E. (2004) Characterization of the histone acetyltransferase (HAT) domain of a bifunctional protein with activable *O*-GlcNAcase and HAT activities. *J. Biol. Chem.* **279,** 53665–53673 CrossRef Medline
39. Hwang, S. Y., Hwang, J. S., Kim, S. Y., and Han, I. O. (2013) O-GlcNAc transferase inhibits LPS-mediated expression of inducible nitric oxide synthase through an increased interaction with mSin3A in RAW264.7 cells. *Am. J. Physiol. Cell Physiol.* **305,** C601–C608 CrossRef Medline
40. Rittirsch, D., Huber-Lang, M. S., Flierl, M. A., and Ward, P. A. (2009) Immunodesign of experimental sepsis by cecal ligation and puncture. *Nat. Protoc.* **4,** 31–36 CrossRef Medline
41. Thimmulappa, R. K., Lee, H., Rangasamy, T., Reddy, S. P., Yamamoto, M., Kensler, T. W., and Biswal, S. (2006) Nrf2 is a critical regulator of the innate immune response and survival during experimental sepsis. *J. Clin. Invest.* **116,** 984–995 CrossRef Medline